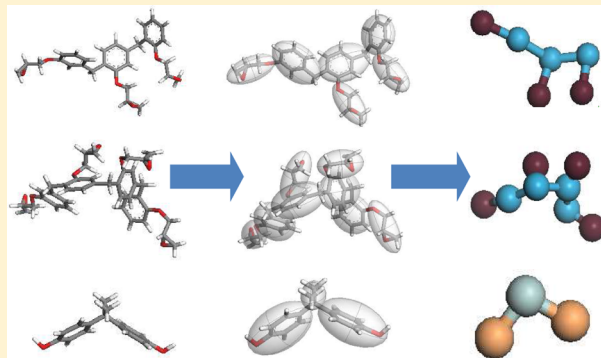


A Coarse-Grained Model for Epoxy Molding Compound

Shaorui Yang,[†] Zhiwei Cui,[†] and Jianmin Qu^{*,†,‡}

[†]Department of Mechanical Engineering and [‡]Department of Civil and Environmental Engineering, Northwestern University, 2145 Sheridan Rd., Evanston, Illinois 60208, United States

ABSTRACT: We present a coarse-grained model for molecular dynamics simulations of an epoxy system composed of epoxy phenol novolac as epoxy monomer and bisphenol-A as the cross-linking agent. The epoxy and hardener molecules are represented as short chains of connected beads, and cross-linking is accomplished by introducing bonds between reactive beads. The interbead potential, composed of Lennard-Jones, bond stretching, and angle bending terms, is parametrized through an optimization process based on a particle swarm optimization method to fit certain key thermomechanical properties of the material obtained from experiments and previous full atomistic simulations. The newly developed coarse-grained model is capable of predicting a number of thermomechanical properties of the epoxy system. The predictions are in very good agreement with available data in the literature. More importantly, our coarse-grained model is capable of predicting tensile failure of the epoxy system, a capability that no other conventional molecular dynamic simulation model has. Finally, our coarse-grained model can speed up the simulations by more than an order of magnitude when compared with traditional molecular dynamic simulations.



1. INTRODUCTION

Epoxy resins, formed by polycondensation of monomers bearing multiple epoxy groups and curing agents with active hydrogens such as hydroxyls and amines, have applications as adhesives, molding compounds, and composites in a variety of fields including electronic packaging, automotive manufacturing, and aerospace industry, due to their excellent thermal and mechanical stability. Characterization of key thermomechanical properties of epoxies is thus of great importance for the validation of structure/device integrity and material design. Besides the conventional trial-and-error procedures which are expensive and time-consuming, computer modeling has been developed into a powerful complementary tool to experiment. Recent developments in molecular level simulations, such as molecular dynamics (MD) simulation, offer the capability to predict material properties, if done properly and with well-parametrized and validated interatomic potential. This has been demonstrated by numerous applications to crystalline materials.^{1–4}

Despite the highly amorphous microstructure and complicated interatomic force fields, polymeric materials have also been extensively examined by molecular modeling. Specifically for chemically cross-linked polymer network, fully atomistic investigations have been practiced based on molecular models constructed through MD simulation of polymerization of physical mixture of monomers into network to study various properties of epoxies.^{5–11} In spite of the extensive use of MD simulations in predicting/reproducing certain properties, the all-atomic models suffer from severe limitations on length and time scales, which restrict their applications in describing

physical processes requiring larger temporal and spatial scales to correctly capture, e.g., mechanical responses of polymers.

Coarse-graining is a method of achieving up-scaling by lumping a group of atoms into a superatom. By doing so, not only can one reduce the system's degree of freedom thus the computation load but also apply larger time step in the MD simulation, due to the softer interparticle interactions. Generally speaking, coarse-graining consists of two steps, namely (i) partitioning the system into bigger structural elements rather than single atoms and (ii) building force field to describe the interbead interactions. The second step, which represents the major challenge in constructing a coarse-grained (CG) model, is highly material and application driven thus does not follow a universal rule.

For coarse-graining, there is a class of methodologies in the literature that focus on accurate matching the materials' structural aspects, such as distribution functions, through iteratively adjusting potential parameters starting from the potential of mean forces derived from the Boltzmann inversion^{12–15} or the inverse Monte Carlo technique.¹⁶ However, as a configurational free energy in the reduced space, the interbead potential's transferability is questionable, in that it is required to be used in the simulation with identical thermodynamic conditions as the force field is fitted to. Furthermore, the resulting potentials are typically rather soft and lack the ability to mimic the mechanical response during

Received: September 17, 2013

Revised: January 20, 2014

Published: January 21, 2014



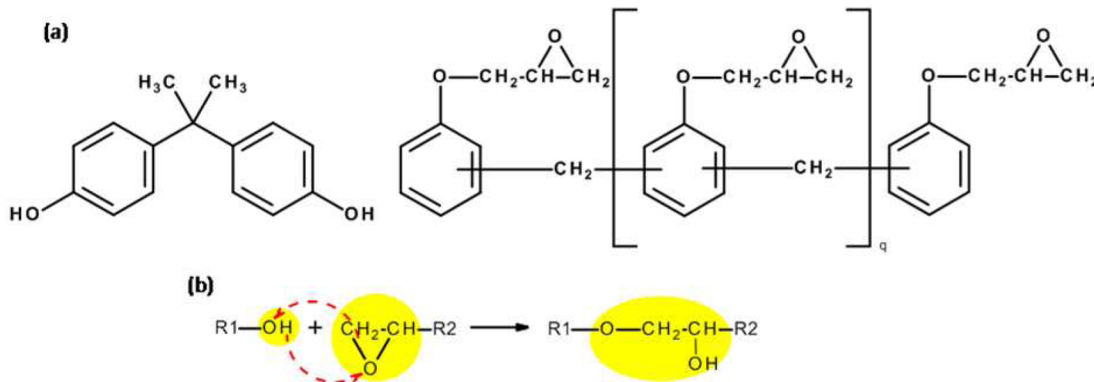


Figure 1. (a) Molecular structures of BPA (left) and EPN1180 (right). (b) Curing reaction mechanism.²⁷

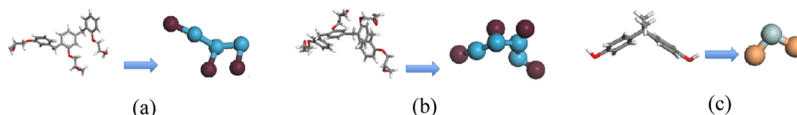


Figure 2. Bead-connector representations of monomers: (a) EPN-3mer, (b) EPN-4mer, and (c) BPA.

large deformation compared to atomic simulations. Usually, when coarse-graining, it is impossible to accurately capture both the structural aspects and thermodynamic properties. Good agreement with one will inevitably lead to poor agreement with the other; thus compromises need to be made. In other words, the ideal CG method depends on what properties one is interested in.

Another philosophy of coarse-graining is to match the materials' physical properties by optimizing parameters of presumed mathematical formulations. For instance, the "MARTINI" force field^{17,18} designed for lipid and surfactant systems was parametrized by reproducing the partitioning free energy between polar and apolar phases of a number of chemical compounds. Similarly, Shinoda et al.¹⁹ developed a coarse-grained potential for surfactant/water systems by fitting density and surface/interfacial tension. Our development for coarse-grained model is based on this latter approach. As will be presented in the following sections, parameters of a few prescribed functional forms are iteratively optimized to reproduce material properties of interests. The versatility of the obtained potential is examined by applying it to structures with a broad range of cross-linking degrees, with emphasis on the ability of correctly capturing cross-link-density's effect on material behavior.

Aside from achieving upscaling in spatial and temporal domains, a strong motivation to the current investigation is to incorporate bond rupture in the force field. This is to model material failure and possible cohesive fracture mechanisms in bimaterials composed of epoxy and inorganic substrates. This capability is missing in most of the fully atomistic models for polymer networks.⁷ From a purely mathematical point of view, the harmonic or quartic-polynomial bond stretching term present in the consistent-valence force field (CVFF²⁰) or the consistent force fields (CFF, e.g., PCFF,^{21,22} COMPASS²³) inherently forbids smooth cutoff of bond energy. Also, simulations of valence bond breakage at atomistic level involve complex re-equilibration of partial charges thus is not practical to implement. On the other hand, a number of works utilizing coarse-grained model with smooth bond cutoff have been conducted to study fracture of epoxy-based materials or other

types of polymer networks.^{24–26} However, these are model materials without correspondence to any real system. Thus, it is desired to have a methodology for efficient development of CG potential that is capable of simulating failure in realistic epoxies or thermosetting polymers.

The rest of the article is organized as follows. In the next section, we will describe the material system to be studied. The partition scheme and interbead interactions and the procedure to construct a highly cross-linked polymer network are also presented. In section 3, we give in detail the algorithm and implementation of the optimization scheme to obtain potential parameters. The parametrized potential is then applied to compute the epoxy molding compound's properties and their correlation to the material's microstructure. A brief summary and some conclusions are given in the last section.

2. COARSE-GRAINED MODEL DEVELOPMENT

2.1. Material System. We choose to model an EPN–BPA epoxy system composed of epoxy phenol novolac (EPN) as epoxy monomer and bisphenol-A (BPA) as the cross-linking agent.²⁷ Their chemical structures are shown in Figure 1a. Note that for this particular formulation the EPN is a mixture of 3mers and 4mers, and the number-averaged functionality is 3.6. The curing reaction between EPN and BPA, as illustrated in Figure 1b, involves opening of the epoxy ring on an EPN monomer and transferring the hydrogen atom from the BPAs' hydroxyl groups to the oxygen atom on the broken ring of the EPN. This frees a carbon atom in the epoxy ring and an oxygen atom in the BPA which are then bonded together to link the EPN and BPA. Polymer chains resulted from two EPNs being connected to one BPA can subsequently be cross-linked due to the multiple functional groups on epoxy monomers.

2.2. Mapping. In building the coarse-grained (CG) models of the above-described tri/tetra-functionalized EPN and BPA monomers, we do not follow the typical scheme of exact one-to-one mapping from a specific chemical moiety to certain bead type, which introduces a variety of different bead types, and thus a large number of parameters for optimization. Instead, we represent the monomer as chains, which maintain similar geometry as their actual atomistic configurations, of connected

beads with unified parameters, i.e., identical mass M , Lennard-Jones potential-well depth ϵ , and diameter σ . The bead-connector representations of the monomers are depicted in Figure 2. Epoxy monomers are simplified as chains of 3 or 4 backbone beads (colored blue in Figure 2a,b), each of which has a reactive branching bead (brown) attached. The hardener monomer possesses two reactive beads (yellow) linked to one center bead (gray). During the cross-linking process, bonds are created between reactive beads on EPNs and BPAs.

The following sections of this article will show that carefully optimized M , ϵ , and σ , along with other potential parameters for bond and angle interactions, enable our coarse-graining model to predict the properties and behavior of realistic epoxy molding compound. A significant advantage of our CG model is the relatively small number of parameters to be determined for a given material system, which allows rapid development of CG models for new materials.

2.3. Interbead Potentials. In the coarse-grained system, nonbonded interactions between beads are described by the Lennard-Jones (LJ) potential

$$U_{\text{LJ}}(r) = 4\epsilon \left[\left(\frac{\sigma}{r} \right)^{12} - \left(\frac{\sigma}{r} \right)^6 \right] \quad (1)$$

In our calculations, the interaction is truncated at the distance of 2.5σ . As previously mentioned, ϵ and σ will be optimized not only to correctly account for the nonbonded interactions but also to provide a good gauge of measurement of the system's actual energy and dimension. Note the LJ interactions are only computed for beads which are separated by at least three bonds.

In our CG model, the bonds between beads are described by a potential function that accounts for bond breakage. It is a sum of the purely repulsive LJ interaction, with a cutoff at $2^{1/6}\sigma$, and a quartic bond potential²⁴

$$\begin{aligned} U_b(r) = & U_0 + k_4(r - r_c)^2(r - b_1 - r_c)(r - b_2 - r_c) \\ & \times H(r_c - r) + 4\epsilon \left[\left(\frac{\sigma}{r} \right)^{12} - \left(\frac{\sigma}{r} \right)^6 + \frac{1}{4} \right] \\ & \times H(2^{1/6}\sigma - r)H(r_c - r) \end{aligned} \quad (2)$$

where $H(x)$ is the Heaviside step function, $k_4 = 1434.3\epsilon/\sigma^4$, $b_1 = -0.7589\sigma$, $b_2 = 0$, and $U_0 = 67.2234\epsilon$.²⁴ The bond extension cutoff r_c will be among the parameters to be fitted. When other parameters are fixed, the effect of r_c on the bond potential is illustrated in Figure 3. It indicates that the equilibrium distance decreases with decreasing cutoff r_c , so does the potential well

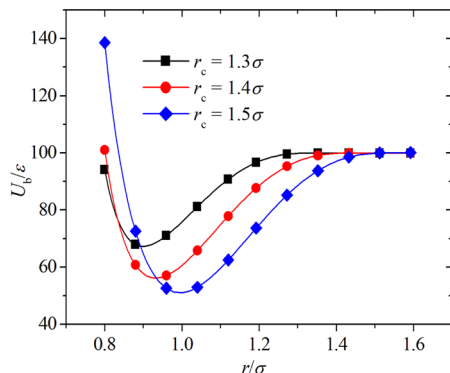


Figure 3. Bond potential curves for different bond extension cutoffs.

depth. At r_c the potential is smoothly truncated, and the bond is removed from the system (bond breakage). Meanwhile, the pair potential (LJ) given by (1) is turned on between the aforebonded pair.

In addition to the LJ and bond terms, angle bending interaction is introduced as a harmonic function:

$$U_a^{(i)}(\theta) = k_\theta^{(i)}(\theta - \theta_0^{(i)})^2 \quad (3)$$

Three angle types are defined. The angle formed by the three beads in a BPA monomer is called type 1, whose equilibrium angle is assumed to be $\theta_0^{(1)} = 100^\circ$. The angle formed by a reactive bead in an EPN and a reactive bead in a BPA is called type 2, whose equilibrium angle is assumed to be $\theta_0^{(2)} = 180^\circ$. All angles formed by beads within each EPN are called type 3, whose equilibrium angle is assumed to be $\theta_0^{(3)} = 180^\circ$. These assumptions on the equilibrium angles are made based on the geometry of the atomistic configurations of the monomers (see Figure 2). The prefactor, $k_\theta^{(i)}$ for $i = 1, 2, 3$ will be determined through the parameter optimization procedure.

2.4. Simulating the Cross-Linking Process. Epoxy-based materials have a percolating network structure formed by chemically curing epoxy and hardener monomers, starting from a liquid mixture. A model for molecular dynamics simulation, either atomistic or coarse-grained, should reflect this unique structural characteristic. To this end, we take a mixture of bead-connector representations of the monomers as described in section 2.2 and randomly seed them into a cubic simulation box with periodic boundary conditions assigned in all three orthogonal directions. The ratio of different types of bead-connector representations corresponds to the stoichiometric ratio of the monomers, i.e., 2:3:9 for 3mer:4mer:BPA. This mixture of bead-connector representations is then equilibrated under constant pressure ensemble at the temperature of $0.8\epsilon/k_B$, where k_B is the Boltzmann constant, with time step of $0.005\tau (\tau = \sigma(M/\epsilon)^{1/2})$ for 1 million steps. The temperature and pressure are controlled by the Nosé–Hoover thermostat and barostat, respectively. The temperature and pressure damping parameters are 200τ and 1000τ , respectively. The same thermostat and barostat are also used in all subsequent MD simulations, unless otherwise indicated. What follows is the dynamic cross-linking process during the constant temperature/pressure MD simulation. In this process, we specify that if an EPN reactive bead is within a 1.3σ radius of a BPA reactive bead, there is a 1% chance that this EPN will form a bond with the BPA. For every 10 MD steps, the system is checked for potential bond formations. In this way, it typically takes 400 000–500 000 MD steps to reach 90% conversion. Because of the 3D periodic nature of the simulation cell, the network actually extends to infinity. In this work, two simulation cells containing 7752 and 45 689 beads, respectively, were constructed. The smaller cell was primarily used for optimizing the parameters in the interbead potential. All material properties were computed using the larger cell.

3. PARAMETER OPTIMIZATION

3.1. Particle Swarm Optimization. As described in the previous sections, a total of seven adjustable parameters, namely, M , ϵ , σ , r_c , $k_\theta^{(1)}$, $k_\theta^{(2)}$, and $k_\theta^{(3)}$, need to be determined for the bond potential in the CG model. This task is accomplished by the particle swarm optimization (PSO) method. The PSO is a population-based stochastic optimization method developed by Kennedy and Eberhart²⁸ for simulating animal social

Table 1. Range of the Search Space of the CG Potential Parameters and Their Optimized Values^a

	M (g/mol)	ϵ (kcal/mol)	σ (Å)	r_c	$k_\theta^{(1)}$	$k_\theta^{(2)}$	$k_\theta^{(3)}$
min	50.0	1.50	4.0	1.25	1.25	1.6	0.2
max	65.0	1.75	5.0	1.4	1.70	2.0	0.5
optimized value	55.565	1.519	4.383	1.343	1.577	1.908	0.403

^a r_c is given in the unit of σ , and $k_\theta^{(1)}$, $k_\theta^{(2)}$, and $k_\theta^{(3)}$ are given in the units of ϵ/rad^2 .

behaviors, e.g., the flying formation of flock of birds or a school of fish when seeking foods. Because of its simple algorithm and fast convergence, the PSO method has been successfully used in many other areas,^{29,30} including optimizing parameters in interatomic potentials in lithium–silicon alloys.^{31,32}

In the PSO method, a population (swarm) of candidate solutions (particles) moves in the search space following some simple mathematical formulas. Their movements are directed by each particle's and the entire swarm's best known positions in the search space. In essence, the method aims to find a solution \mathbf{x}_0 that satisfies the condition of $f(\mathbf{x}_0) \leq f(\mathbf{x})$ for any particle \mathbf{x} in the search space. A typical PSO procedure includes the following steps:

(1) Initialize the i th particle's position \mathbf{x}_i and its own best known position \mathbf{p}_i to \mathbf{x}_i ; update the global best position \mathbf{g} to \mathbf{p}_i if $f(\mathbf{p}_i) \leq f(\mathbf{g})$ holds, where f is the objective function; initialize the i th particle's velocity \mathbf{v}_i .

(2) Update the i th particle's velocity \mathbf{v}_i and its position \mathbf{x}_i ($\mathbf{x}_i \leftarrow \mathbf{x}_i + \mathbf{v}_i$) accordingly; set \mathbf{p}_i to \mathbf{x}_i if $f(\mathbf{x}_i) \leq f(\mathbf{p}_i)$ is satisfied and \mathbf{g} to \mathbf{p}_i if $f(\mathbf{p}_i)$ is less than or equal to $f(\mathbf{g})$.

(3) Repeat (2) until convergence criterion is met.

3.2. Implementation. In the current investigation, a particle corresponds to a set of candidate parameters in our CG potential, i.e., $\mathbf{x} = \{M, \epsilon, \sigma, r_c, k_\theta^{(1)}, k_\theta^{(2)}, k_\theta^{(3)}\}$. The objective function is defined as

$$f(\mathbf{x}) = \sum_{i=1}^N \left[\frac{g_i(\mathbf{x})}{y_i} - 1 \right]^2 \quad (4)$$

where y_i ($i = 1, 2, \dots, N$) is a set of known physical properties of the EPN–BPA epoxy system considered here, and $g_i(\mathbf{x})$ is the same set of physical properties calculated by our CG model using the potentials described by eqs 1–3 with the set of parameters \mathbf{x} . The goal of the optimization is to select a set \mathbf{x}_0 so that $f(\mathbf{x}_0) \leq f(\mathbf{x})$ for all \mathbf{x} in the search space. In theory, the larger the N , the more accurate the solution will be. Similarly, the larger of the search space, the more global of the solution will be. Both, of course, will result in more extensive computations. In this study, we strike a balance between accuracy and efficiency by using $N = 8$ parameters including the glass transition temperature, room temperature density, modulus, and Poisson's ratio for the 90% cross-linked and precured systems. For consistency, we used the values of these properties calculated by the full MD simulations from our previous work.¹⁰ In determining the size of the search space, we used an empirical approach by conducting several parametric studies to observe dependency of the physical properties on these potential parameters, from which the range of values of these potential parameters can be estimated, since the range of values of these physical properties are known. The size of the search space so selected is listed in Table 1.

To start the optimization, each parameter is given an initial value randomly within its search space. Then, CG simulations are conducted on two models; one is cross-linked, and the other is not. The two models are first separately geometry-

optimized using energy minimization and equilibrated under constant pressure CGMD simulation at elevated temperature. Then a few CGMD simulations were conducted to obtain their physical properties. The glass transition temperatures were computed from the volume versus temperature data in cooling simulations (shown in Figure 4a), as the intersection point of the bilinear function used to fit the raw data. Figure 4b illustrates the constant pressure simulation at room temperature, from which the densities of the two models were calculated. The elastic constants, including Young's modulus and Poisson's ratio, were extracted from simulated uniaxial tension (Figure 4c,d), using linear regression over the stress vs strain and the axial strain vs lateral strain data within the linear elastic regime. The computed physical properties are in the LJ unit system, since the correct values of M , ϵ , and σ were yet unknown at this stage. They are converted to real physical units using the (guessed) values of M , ϵ , and σ :

$$\begin{aligned} T_g^{\text{real}} &= T_g^{\text{LJ}} \epsilon / k_B, & d^{\text{real}} &= d^{\text{LJ}} M / \sigma^3 \\ E^{\text{real}} &= E^{\text{LJ}} \epsilon / \sigma^3, & \nu^{\text{real}} &= \nu^{\text{LJ}} \end{aligned} \quad (5)$$

where the superscripts "real" and "LJ" are for real physical and LJ units.

Once the physical properties were calculated from eq 5, the objective function in eq 4 can be evaluated and used as criterion for update of local and/or global best known positions of particles. The above-described process repeats until a good set of parameters are found, i.e., $f(\mathbf{x}_0) \leq 0.022$. The actual process was implemented and carried out using a code originally developed by Cui et al.^{31,32} for the Li–Si systems and modified to our problem, which consists of the LAMMPS software for CG MD simulations, postprocessing of data to compute the physical properties, and the PSO algorithm for optimization.

The optimized values of the potential parameters are listed in Table 1. Table 2 provides the comparison between the physical properties calculated using the CG potential parameters and their targeted values from the MD simulations.¹⁰ We stopped the optimization when the objective function reaches an acceptable value, $f(\mathbf{x}_0) \leq 0.0216$. This is a compromise between accuracy and efficiency.

To close this section, we note that the bond potential given by (2) was motivated by the earlier works in the subject such as.^{24–26} As mentioned in section 1, these earlier works proposed the functional form of the potential but did not associate the parameters in the bond potential with any specific material. Thus, their potentials cannot be used to simulate the behavior of any realistic material. In this work, we proposed an effective method to optimize these parameters for a given material of interest. By using this method, optimal values of these parameters were obtained for a commercial epoxy molding compound. Such parametrized bond potential enables the simulation of the properties and mechanical behavior of a realistic epoxy mold compound. The proposed parametrization method is rather general and can be used for other epoxy systems. Another improvement over the earlier works, e.g. refs

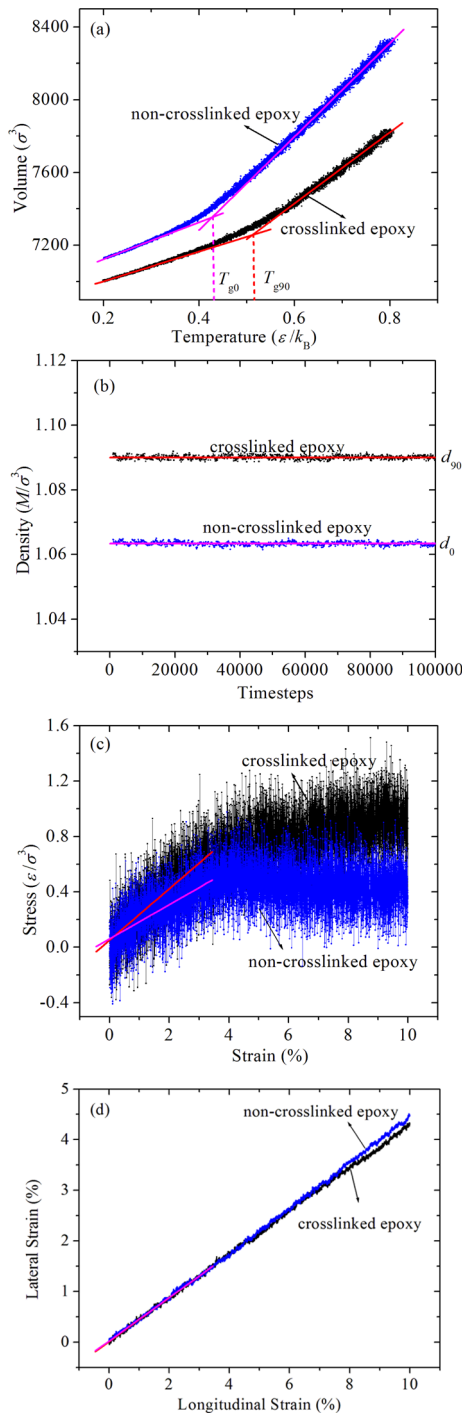


Figure 4. Physical properties of the two models (precured and cross-linked with conversion of 90%). (a) T_g 's are obtained as the intersection of bilinear functions used to fit volume versus temperature curves. (b) Densities are obtained as the averaged value over the duration from $N = 50\,000$ to $N = 100\,000$, where N is the number of time steps. (c) Young's moduli are obtained as the slope of the linear portion of the stress-strain curve. (d) Poisson's ratios are obtained as the slope of the linear function fitting the lateral–axial strain data.

24–26, is the inclusion of angle bending terms (3) in the overall interbead potential. The bending terms describe the angular energy between a pair of neighboring beads. We found that inclusion of such angle bending terms is essential to fully describe the interactions among the beads.

4. RESULTS AND DISCUSSION

Using the CG model developed here together with the optimized parameters shown in Table 1, we carried out CGMD simulations on the epoxy system discussed in section 2.1 to obtain certain thermomechanical properties and their dependence on the degree of cross-linking. The simulation cell is a cube measured ~ 152 Å in each direction and contains 45 689 beads. The precured system containing fluidic mixture of monomers was first equilibrated under constant pressure ensemble at 610 K for 10^6 steps with a time step of 5 fs. During the subsequent 10^6 step NPT simulation, bonds were formed conditionally with a probability of 0.01 between reactive beads on EPN and BPA monomers, provided they are within the bond-formation cutoff of 5.7 Å (see the discussions in section 2.4). The dynamic cross-linking process proceeded until the desired rate of conversion was reached. In this work, systems with 25%, 50%, 75%, and 90% were considered.

4.1. Glass Transition. The cross-linked epoxy molding compound was further equilibrated under NPT ensemble at high temperature (610 K) before cooling simulation started. The CGMD cooling process decreases the temperature continuously from 610 to 150 K within 4×10^6 steps. With the time step of 5 fs, the cooling rate is 2.3×10^{10} K/s. In Figure 5 we plotted the specific volume versus temperature relationship for 90%, 50%, and 0% cross-linked epoxy systems. The glass transition temperature T_g is defined as the temperature at which the specific volume versus temperature curve shows a kink. It is seen from Figure 5 that T_g for the 90% and 0% cross-linked systems are 401 and 312 K, respectively. These values are in good agreement with those obtained from the full MD simulated results.¹⁰ This is not surprising because T_g at these two conversion rates is one of the physical parameters used in optimizing the CG potential parameters. To verify that the validity of our CG model predictions at other conversion rates, we plotted in Figure 6 the comparison between our CG results and the MD results.¹⁰ The error bars are associated with different choices of temperature ranges while doing bilinear regression. It is seen that the T_g –conversion relationship predicted by the newly developed CGMD is very close to that predicted by conventional full MD simulations.¹⁰ This shows that our CG model and potential can correctly capture the property transition with the progress of cross-linking.

4.2. Elastic Constants. Using the CG model developed here, we simulate the elastic constants and their dependence on material microstructure and temperature in this section. To this end, we will use the fluctuation formula for the stiffness matrix^{33,34}

$$C_{ijkl} = \langle \sigma_{ij} \epsilon_{mn} \rangle \langle \epsilon_{mn} \epsilon_{kl} \rangle^{-1} \quad (6)$$

where the angle brackets represent ensemble average, σ_{ij} and ϵ_{ij} are respectively the virial stress and strain tensors given by

$$\sigma_{ij} = \frac{1}{V} \left[\sum_{\alpha} m_{\alpha} (v_{\alpha})_i (v_{\alpha})_j - \sum_{\beta > \alpha} \frac{\partial U}{\partial r_{\alpha\beta}} \frac{(r_{\alpha\beta})_i (r_{\alpha\beta})_j}{r_{\alpha\beta}} \right] \quad (7)$$

$$\epsilon_{ij} = \frac{1}{2} [\langle h \rangle_{ik}^{-T} h_{kl}^T h_{lm} \langle h \rangle_{mj}^{-1} - \delta_{ij}] \quad (8)$$

In eq 7, subscripts α and β stand for the α th and β th atoms; m , v , r , and U are atomic mass, velocity, distance and system's potential energy, respectively. In eq 8, h is the scaling matrix $h =$

Table 2. Comparison between Material Properties Calculated by the CG Model and MD Simulations^a

	$T_g^{(90)}$	$T_g^{(0)}$	$d^{(90)}$	$d^{(0)}$	$E^{(90)}$	$E^{(0)}$	$\nu^{(90)}$	$\nu^{(0)}$
MD results	404	304	1.172	1.111	2.517	1.836	0.375	0.382
CG results	402.8	317.6	1.183	1.156	2.489	1.868	0.412	0.416

^aSuperscripts (90) and (0) stands for 90% cross-linked and non-cross-linked models, respectively. Units for temperature, density, and modulus are in kelvin (K), g/cm³, and GPa, respectively.

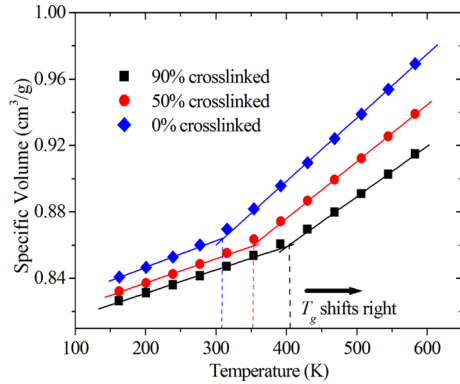


Figure 5. Specific volume versus temperature relationships for systems with different conversions using the optimized CG potential parameters.

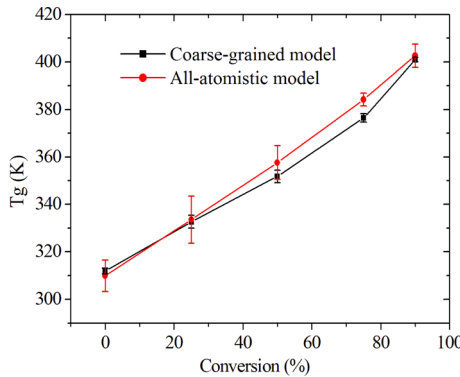


Figure 6. Glass transition temperature versus conversion relationships obtained from CG and full MD simulations.¹⁰

$\{\vec{a}, \vec{b}, \vec{c}\}$ with \vec{a} , \vec{b} , and \vec{c} being the basis vectors of the simulation cell.

In order to correctly calculate values of stiffness matrix and the elastic constants, the linear elastic assumption needs to be satisfied. That means the strains and their fluctuations should be sufficiently small. Furthermore, it is well-known that polymers become very soft when temperature goes above T_g since the material transits into a rubbery phase. In the rubbery phase, it is rather difficult to obtain the strain components accurately. To solve this problem, we will adopt the elastic bath method to constraint the material in the linear elastic state. The method immerses the CGMD simulation cell into an elastic bath with certain stiffness matrix C_{ijkl}^b . The system's Hamiltonian is given by³³

$$H = \sum_{\alpha} \frac{\vec{p}_{\alpha}^T G^{-1} \vec{p}_{\alpha}}{2m_{\alpha}} + U(\vec{q}, G) + \frac{1}{2} \langle V \rangle C_{ijkl}^b \epsilon_{ij} \epsilon_{kl} \quad (9)$$

where \vec{p}_{α} is the α th atom's linear momentum, $G = h^2 \mathbf{h}$ is the metric tensor, and V is the simulation cell's volume. The stiffness tensor for the cell/bath system is

$$\begin{aligned} C_{ijkl}^t &= \langle (\sigma_{ij} + C_{ijkl}^b \epsilon_{kl}) \epsilon_{mn} \rangle \langle \epsilon_{mn} \epsilon_{kl} \rangle^{-1} = \langle \sigma_{ij} \epsilon_{mn} \rangle \langle \epsilon_{mn} \epsilon_{kl} \rangle^{-1} \\ &+ C_{ijkl}^b \end{aligned} \quad (10)$$

where C_{ijkl}^b is elastic stiffness tensor of the elastic bath. Thus, the stiffness matrix for the simulation cell is

$$C_{ijkl} = \langle \sigma_{ij} \epsilon_{mn} \rangle \langle \epsilon_{mn} \epsilon_{kl} \rangle^{-1} = C_{ijkl}^t - C_{ijkl}^b \quad (11)$$

In the Voigt notation, an isotropic elastic bath can be described by its Lamé constants λ^b and μ^b

$$C_{11}^b = \lambda^b + 2\mu^b, \quad C_{12}^b = \lambda^b, \quad C_{44}^b = \mu^b, \quad \text{others} = 0 \quad (12)$$

which can be arbitrarily chosen to ensure the strain components in the simulation cell are small.

The above fluctuation method was implemented in our CGMD model under NPT simulations using the Nosé–Hoover thermostat, and the Parrinello–Rahman barostat, which allow all 6 degrees of freedom of the simulation box to be independently adjusted, was conducted for 5×10^8 steps. The stress and strain tensors were extracted from the CGMD runs every 100 steps. At temperatures lower than 400 K (T_g) the elastic bath method was not invoked, since the material is still glassy and strain was sufficiently small without additional constraints. At 400 K and higher temperatures, elastic bath is added to ensure all strain components are less than 1%. Figure 7a,b plots the variation of moduli and Poisson's ratio with temperature for the 90% cross-linked epoxy model.

Figure 7 clearly shows the transition of moduli and Poisson's ratio around the glass transition temperature; namely, the Young's and shear moduli show drastic drop of 2 orders of magnitude starting from approximately 400 K, indicating significant softening of the epoxy molding compound in its rubbery state. In the meantime, the Poisson's ratio rises up to approaching 0.5, indicating that the solid is transitioning into an incompressible fluid. At the two highest temperatures simulated (460 and 480 K), the Poisson's ratio falls in the range of 0.49–0.5, which is typical for the rubbery state of thermosetting polymers. In contrast, the bulk modulus remains relatively unchanged even at temperature much higher than 400 K which, again, is typical for the rubbery-state thermosetting polymers.

We note that the glass transition temperature can also be defined by the temperature at which the elastic moduli drop significantly. Using this definition, the T_g for the epoxy at hand would be about 400 K, which is consistent with the value obtained in section 4.1 using the specific volume versus temperature relationship.

To better understand the structure–property relationship, the Young's modulus (E) versus temperature curves for different conversion rates are shown in Figure 8. It is seen that Young's modulus for epoxy systems with different conversion rates all exhibit a drop of 2 orders of magnitude around the glass transition temperature. The glass transition temperatures obtained from Figure 8 are consistent with those obtained in section 4.1 using the specific volume versus temperature relationship. This further validated our CG model

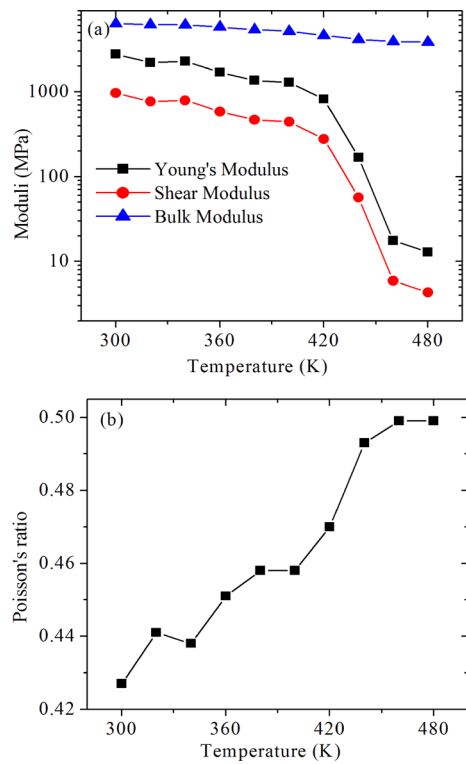


Figure 7. (a) Moduli and (b) Poisson's ratio versus temperature relationships for the 90% cross-linked epoxy using our CGMD model and potential.

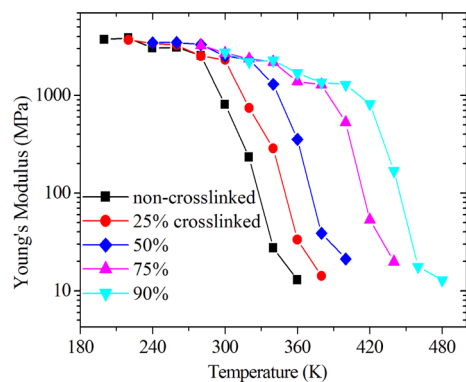


Figure 8. Young's modulus versus temperature relationships for epoxies with different conversion rates.

in terms of its capability to predict the correct thermomechanical properties for epoxies with a wide range of cross-link density.

4.3. Deformation and Failure Behavior. To investigate the deformation and failure behavior of the epoxy molding compound, CGMD simulations of uniaxial tension were conducted. For these simulations, we used a bigger simulation cell consisting 209 304 beads. The cubic cell measures 253 Å in each direction. To simulate uniaxial tension, the cell was stretched along one direction, while the pressure on the other two perpendicular directions was kept zero using the Nosé–Hoover barostat. Three different strain rates were used, $10^8/\text{s}$, $5 \times 10^8/\text{s}$, and $10^9/\text{s}$.

The simulated uniaxial stress–strain curves are presented in Figure 9. It is seen that the general behavior of the stress–strain curves is similar under different loading rates. They all show

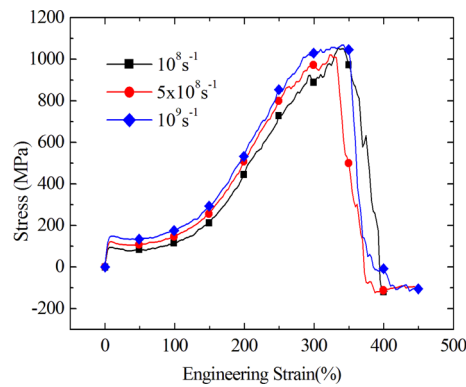


Figure 9. Stress–strain curves for the uniaxial tensile simulation using different strain rates.

four distinct stages. In the first stage, the stress is almost linearly related to the strain up to the point of yielding, which will be called the yield strength. We see that the yield strength varies from 94 to 147 MPa when the strain rate increases from $10^8/\text{s}$ to $10^9/\text{s}$. From yielding to about 50% strain is the second stage, where the material undergoes a slight strain softening. The primary mechanism for such a phenomenon is the relaxation of polymer conformations as well as the reorientation of polymer strands, both intrinsically sluggish processes. During this stage, the polymer strands seek a more energetically favorable configuration in the conformational space that results in a softening behavior.³⁵ Following the strain softening is the third stage, where the material experiences strain hardening. The hardening process is accompanied by orientating the polymer network strands along the loading direction. Strands are successively pulled taut, and stress rises sharply until the ultimate strength is reached. In the fourth and final stage, the stress drops to zero almost instantaneously, indicating a brittle-like failure.

To better understand mechanisms behind the stress–strain behavior, we show in Figure 10 the fraction of broken bonds

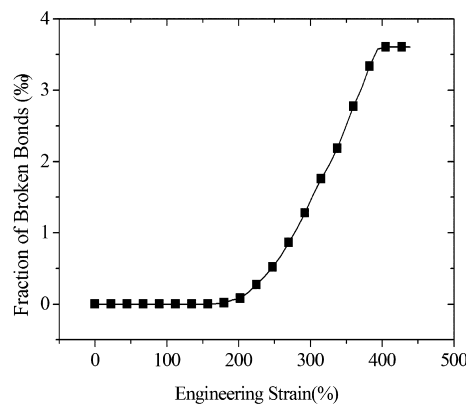


Figure 10. Number fraction of broken bonds versus strain.

(out of originally 217 457 bonds). It is clear that most of the bonds remain intact until the strain is more than 150%. Since the stress only experiences mild hardening before this strain, one may conclude that the deformation over this strain range is mainly due to reorientation of polymer strands from their initial coiled state to a more linear state. After about 200% strain, bonds start to break as the deformation increases. The number of bonds rupture is almost linearly proportional to the strain

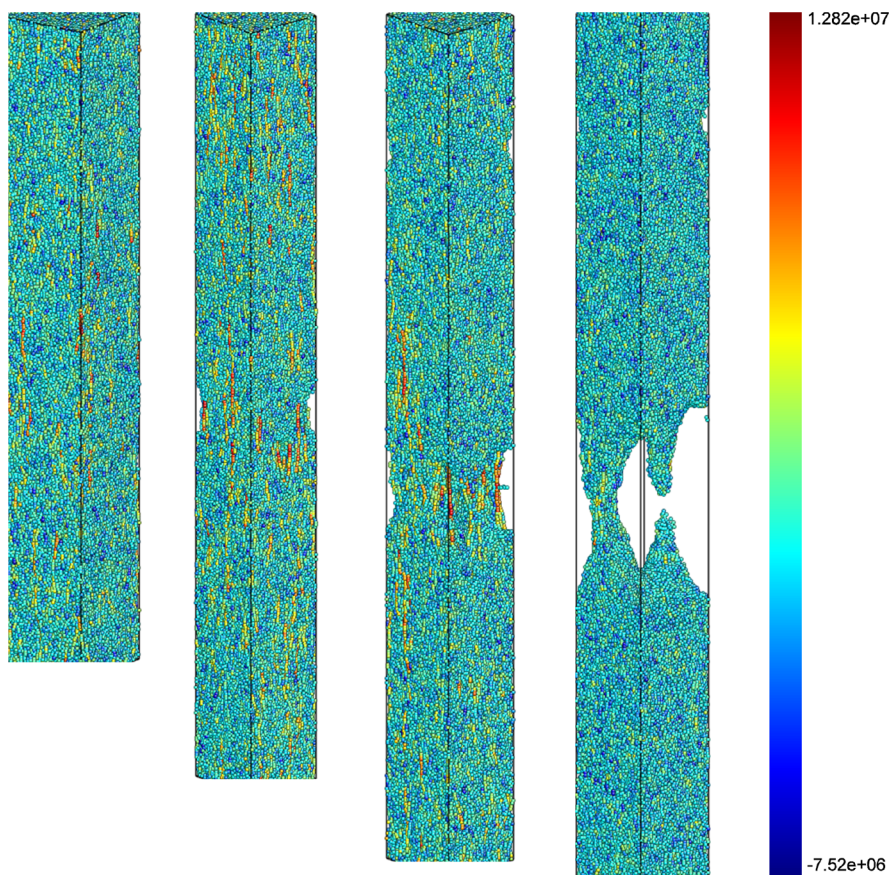


Figure 11. Snapshots of deformed configurations during the uniaxial tension for strains of (from left to right): 259%, 348%, 372%, and 394%. Beads are colored according to their virial stress along the loading direction. The color bar is shown right to the last snapshot.

(see Figure 10). In conjunction with the near linear stress-strain relationship in the third stage of the uniaxial tension shown in Figure 9, one may conclude that the load is primarily carried by the stretching of the bonds.

In addition, since the bond “strength” between two beads is characterized by the maximum distance between the beads, the linear relationship between the number of bond ruptures, and the applied strain means that the polymer strands continue to realign themselves as the strain increases so that more and more bonds are reaching their “strength”. To illustrate the realignment of the polymer strands, snapshots of deformed configurations, with beads colored by virial stress along the loading direction, are presented in Figure 11. In the leftmost snapshot, some of the highly aligned polymer strands are seen as those chains with colors corresponding to the highest color-map scales. These strands experience large stress and are the most probable locations for bond ruptures. The accumulative bond rupture process will eventually lead to localization, as can be observed in the second snapshot of Figure 11. Roughly at the same strain, the epoxy reaches its ultimate strength. In this snapshot one can also find a bundle of deep colored, thus highly stressed, strands concentrated near the failure site. This stress concentration leads to rapid scission of a large number of strands near the failure surface. To quantify the localization, we plotted in Figure 12 the spatial distribution of percentage of broken bonds at different strain levels.

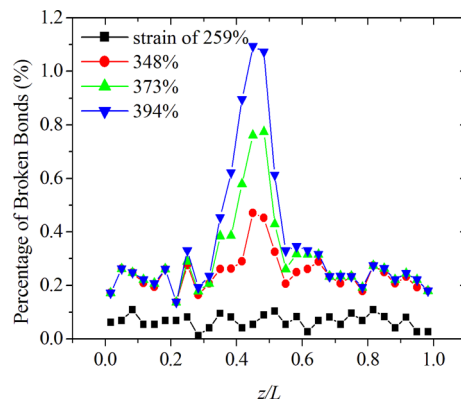


Figure 12. Spatial distribution of percentage of broken bonds at different strain levels.

Comparison of Figure 10 with Figure 12 shows that the rate of overall bond rupture remains almost constant in the strain range of 200%–400%, but the increase occurs only locally near the failure surface.

The predicted ultimate failure strength is about 1 GPa, which is an order of magnitude higher than experimentally measured strength of epoxy-based thermosetting polymers. This discrepancy may come from several factors such as the pristine state of the CGMD sample (defect free) and the high strain rate used in the CGMD simulations. These drawbacks are intrinsic to such fine scale simulations. For example, Gall et al.³⁶ reported the debonding strength of Al-Si bimaterial to be 20 GPa, which is much higher than the experimentally measured ultimate tensile

strength (~ 200 MPa) of cast Al–Si alloy.^{37,38} In the work by Panico et al.,³⁹ the authors also predicted very high ultimate strength for cross-linked polymers, $\sim 5.5\epsilon/\sigma^3$ in the LJ unit. In the LJ unit, our simulated the strength is $8.5\epsilon/\sigma^3$, consistent with ref 39.

5. CONCLUSIONS

In the current investigation, we developed a coarse-grained model for an epoxy molding compound. The coarse-grained model is based on a bead–spring representation of the constitutive monomers of the epoxy system. The interactions between beads are represented by the interbead potentials consisting of a Lennard-Jones potential, a quartic function to capture bond stretch and strength, and harmonic functions to describe angle bonds. By using the particle swarm optimization technique,^{31,32} parameters in the interbead potential function were optimized through fitting certain key thermomechanical properties calculated from our previous atomistic MD studies.¹⁰ We demonstrated that the newly developed coarse-grained model is able to reproduce, in good agreement with atomic MD results, density, glass transition temperature, and elastic constants as well as these properties' temperature and structural dependence.

One significant advantage of the newly developed coarse-grained model is its ability to simulate bond breakage, which enables the simulation of polymer failure. No interatomic potential is currently available in the open literature that is capable of predicting failure of polymer materials. Taking advantage of the new capabilities, we simulated the uniaxial tension behavior of the epoxy compound. We found that, under the uniaxial stress condition, the polymer network experiences continuous orientation and scission of epoxy network strands, which eventually leads to localization of bond rupture and failure.

Finally, it is important to point out that the coarse-grained model significantly speeds up the simulation and allows us to simulate material size that is not feasible in conventional MD simulations. For example, for a simulation box of $250 \times 250 \times 250 \text{ \AA}^3$, it takes our CG model about 1 min of CPU time on a cluster of 108 Intel processors for each 10^4 time steps. On the other hand, even for a much smaller simulation box of $100 \times 100 \times 100 \text{ \AA}^3$, it would take a conventional MD model more than 20 min of CPU to do the same.

AUTHOR INFORMATION

Corresponding Author

*E-mail j-qu@northwestern.edu, Ph 847-467-4528 (J.Q.).

Notes

The authors declare no competing financial interest.

ACKNOWLEDGMENTS

The work was supported in part by a grant from NSF (CMMI-1200075).

REFERENCES

- (1) Leach, A. M.; McDowell, M.; Gall, K. Deformation of Top-Down and Bottom-up Silver Nanowires. *Adv. Funct. Mater.* **2007**, *17*, 43–53.
- (2) Lee, B.-J.; Shim, J.-H.; Baskes, M. I. Semiempirical Atomic Potentials for the Fcc Metals Cu, Ag, Au, Ni, Pd, Pt, Al, and Pb Based on First and Second Nearest-Neighbor Modified Embedded Atom Method. *Phys. Rev. B* **2003**, *68*, 144112-1–144112-11.
- (3) Mishin, Y.; Mehl, M. J.; Papaconstantopoulos, D. A.; Voter, A. F.; Kress, J. D. Structural Stability and Lattice Defects in Copper: Ab Initio, Tight-Binding, and Embedded-Atom Calculations. *Phys. Rev. B* **2001**, *63*, 224106-1–224106-15.
- (4) Park, H. S.; Zimmerman, J. A. Modeling Inelasticity and Failure in Gold Nanowires. *Phys. Rev. B* **2005**, *72*, 054106-1–054106-9.
- (5) Bandyopadhyay, A.; Valavalas, P. K.; Clancy, T. C.; Wise, K. E.; Odegard, G. M. Molecular Modeling of Crosslinked Epoxy Polymers: The Effect of Crosslink Density on Thermomechanical Properties. *Polymer* **2011**, *52*, 2445–2452.
- (6) Komarov, P. V.; Chiu, Y. T.; Chen, S. M.; Khalatur, P. G.; Reineker, P. Highly Cross-Linked Epoxy Resins: An Atomistic Molecular Dynamics Simulation Combined with a Mapping/Reverse Mapping Procedure. *Macromolecules* **2007**, *40*, 8104–8113.
- (7) Strachan, A.; Li, C. Y. Molecular Dynamics Predictions of Thermal and Mechanical Properties of Thermoset Polymer Epon862/Detda. *Polymer* **2011**, *52*, 2920–2928.
- (8) Varshney, V.; Patnaik, S. S.; Roy, A. K.; Farmer, B. L. A Molecular Dynamics Study of Epoxy-Based Networks: Cross-Linking Procedure and Prediction of Molecular and Material Properties. *Macromolecules* **2008**, *41*, 6837–6842.
- (9) Wu, C. F.; Xu, W. J. Atomistic Molecular Modelling of Crosslinked Epoxy Resin. *Polymer* **2006**, *47*, 6004–6009.
- (10) Yang, S.; Qu, J. Computing Thermomechanical Properties of Crosslinked Epoxy by Molecular Dynamic Simulations. *Polymer* **2012**, *53*, 4806–4817.
- (11) Yarovsky, I.; Evans, E. Computer Simulation of Structure and Properties of Crosslinked Polymers: Application to Epoxy Resins. *Polymer* **2002**, *43*, 963–969.
- (12) Shelley, J. C.; Shelley, M. Y.; Reeder, R. C.; Bandyopadhyay, S.; Klein, M. L. A Coarse Grain Model for Phospholipid Simulations. *J. Phys. Chem. B* **2001**, *105*, 4464–4470.
- (13) Vettorel, T.; Meyer, H. Coarse Graining of Short Polyethylene Chains for Studying Polymer Crystallization. *J. Chem. Theory Comput.* **2006**, *2*, 616–629.
- (14) Fukunaga, H.; Takimoto, J.; Doi, M. A Coarse-Graining Procedure for Flexible Polymer Chains with Bonded and Nonbonded Interactions. *J. Chem. Phys.* **2002**, *116*, 8183–8190.
- (15) Li, Y.; Tang, S.; Abberton, B. C.; Kroger, M.; Burkhardt, C.; Jiang, B.; Papakonstantopoulos, G. J.; Poldneff, M.; Liu, W. K. A Predictive Multiscale Computational Framework for Viscoelastic Properties of Linear Polymers. *Polymer* **2012**, *53*, 5935–5952.
- (16) Murtola, T.; Falck, E.; Patra, M.; Karttunen, M.; Vattulainen, I. Coarse-Grained Model for Phospholipid/Cholesterol Bilayer. *J. Chem. Phys.* **2004**, *121*, 9156–9165.
- (17) Marrink, S. J.; de Vries, A. H.; Mark, A. E. Coarse Grained Model for Semiquantitative Lipid Simulations. *J. Phys. Chem. B* **2004**, *108*, 750–760.
- (18) Marrink, S. J.; Risselada, H. J.; Yefimov, S.; Tieleman, D. P.; de Vries, A. H. The Martini Force Field: Coarse Grained Model for Biomolecular Simulations. *J. Phys. Chem. B* **2007**, *111*, 7812–7824.
- (19) Shinoda, W.; Devane, R.; Klein, M. L. Multi-Property Fitting and Parameterization of a Coarse Grained Model for Aqueous Surfactants. *Mol. Simul.* **2007**, *33*, 27–36.
- (20) Dauberosguthorpe, P.; Roberts, V. A.; Osguthorpe, D. J.; Wolff, J.; Genest, M.; Hagler, A. T. Structure and Energetics of Ligand-Binding to Proteins - Escherichia-Coli Dihydrofolate Reductase Trimethoprim, a Drug-Receptor System. *Proteins: Struct., Funct., Genet.* **1988**, *4*, 31–47.
- (21) Sun, H. Force-Field for Computation of Conformational Energies, Structures, and Vibrational Frequencies of Aromatic Polyesters. *J. Comput. Chem.* **1994**, *15*, 752–768.
- (22) Sun, H.; Mumby, S. J.; Maple, J. R.; Hagler, A. T. An Ab Initio Cff93 All-Atom Force Field for Polycarbonates. *J. Am. Chem. Soc.* **1994**, *116*, 2978–2987.
- (23) Sun, H. Compass: An Ab Initio Force-Field Optimized for Condensed-Phase Applications—Overview with Details on Alkane and Benzene Compounds. *J. Phys. Chem. B* **1998**, *102*, 7338–7364.
- (24) Lorenz, C. D.; Stevens, M. J.; Wool, R. P. Fracture Behavior of Triglyceride-Based Adhesives. *J. Polym. Sci., Polym. Phys.* **2004**, *42*, 3333–3343.

- (25) Stevens, M. J. Interfacial Fracture between Highly Cross-Linked Polymer Networks and a Solid Surface: Effect of Interfacial Bond Density. *Macromolecules* **2001**, *34*, 2710–2718.
- (26) Tsige, M.; Stevens, M. J. Effect of Cross-Linker Functionality on the Adhesion of Highly Cross-Linked Polymer Networks: A Molecular Dynamics Study of Epoxies. *Macromolecules* **2004**, *37*, 630–637.
- (27) Sadeghinia, M.; Jansen, K. M. B.; Ernst, L. J. Characterization and Modeling the Thermo-Mechanical Cure-Dependent Properties of Epoxy Molding Compound. *Int. J. Adhes. Adhes.* **2012**, *32*, 82–88.
- (28) Kennedy, J.; Eberhart, R. *Particle Swarm Optimization; Neural Networks*, 1995. Proceedings IEEE International Conference on Nov/Dec 1995; pp 1942–1948.
- (29) Begambre, O.; Laier, J. E. A Hybrid Particle Swarm Optimization - Simplex Algorithm (Psos) for Structural Damage Identification. *Adv. Eng. Softw.* **2009**, *40*, 883–891.
- (30) Lee, W. S.; Chen, Y. T.; Wu, T. H. Optimization for Ice-Storage Air-Conditioning System Using Particle Swarm Algorithm. *Appl. Energy* **2009**, *86*, 1589–1595.
- (31) Cui, Z. W.; Gao, F.; Cui, Z. H.; Qu, J. M. Developing a Second Nearest-Neighbor Modified Embedded Atom Method Interatomic Potential for Lithium. *Model. Simul. Mater. Sci. Eng.* **2012**, *20*, 015014–1–015014–12.
- (32) Cui, Z. W.; Gao, F.; Cui, Z. H.; Qu, J. M. A Second Nearest-Neighbor Embedded Atom Method Interatomic Potential for Li-Si Alloys. *J. Power Sources* **2012**, *207*, 150–159.
- (33) Cui, Z. W.; Sun, Y.; Li, J.; Qu, J. M. Combination Method for the Calculation of Elastic Constants. *Phys. Rev. B* **2007**, *75*, 214101-1–214101-6.
- (34) Li, J.; Sun, Y.; Cui, Z. W.; Zeng, F. L. Least Square Method for the Calculation of Elastic Constants. *Comput. Phys. Commun.* **2011**, *182*, 1447–1451.
- (35) Cui, Z.; Brinson, L. C. Thermomechanical Properties and Deformation of Coarse-Grained Models of Hard-Soft Block Copolymers. *Phys. Rev. E* **2013**, *88*, 022602-1–022602-10.
- (36) Gall, K.; Horstemeyer, M. F.; Van Schilfgaarde, M.; Baskes, M. I. Atomistic Simulations on the Tensile Debonding of an Aluminum-Silicon Interface. *J. Mech. Phys. Solids* **2000**, *48*, 2183–2212.
- (37) Dighe, M. D.; Gokhale, A. M. Relationship between Microstructural Extremum and Fracture Path in a Cast Al-Si-Mg Alloy. *Scr. Mater.* **1997**, *37*, 1435–1440.
- (38) Samuel, A. M.; Samuel, F. H. A Metallographic Study of Porosity and Fracture-Behavior in Relation to the Tensile Properties in 319.2 End-Chill Castings. *Metall. Mater. Trans. A* **1995**, *26*, 2359–2372.
- (39) Panico, M.; Narayanan, S.; Brinson, L. C. Simulations of Tensile Failure in Glassy Polymers: Effect of Cross-Link Density. *Model. Simul. Mater. Sci. Eng.* **2010**, *18*, 055005-1–055005-11.